Electromagnetic Induction Spectroscopy

I.J. Won, Dean Keiswetter, and Elena Novikova
Geophex, Ltd.

ABSTRACT

An object, made partly or wholly of metals, has a distinct combination of electrical conductivity, magnetic permeability, and geometrical shape and size. When the object is exposed to a low-frequency electromagnetic field, it produces a secondary magnetic field. By measuring the broadband spectrum of the secondary field, we obtain a distinct spectral signature that may uniquely identify the object. Based on the response spectrum, we attempt to "fingerprint" the object. This is the basic concept of *Electromagnetic Induction Spectroscopy (EMIS)*.

EMIS technology can be particularly useful for detecting buried landmines and unexploded ordnance. By fully characterizing and identifying an object without excavation, we should be able to reduce significantly the number of false targets. EMIS is applicable to many other problems where target identification and recognition (without intrusive search) are important. For instance, an advanced EMIS device at an airport security gate may be able to identify a particular weapon according to its maker and type. Other potential applications may include industrial sorting processes and robotics.

Introduction

When an electrically conductive and/or magnetically permeable object is placed in a time-varying electromagnetic field, a system of induced current flows through the object. By observing the small secondary magnetic field emanating from the induced current, we attempt to detect the object; this is the foundation of the time-proven electromagnetic induction (EMI) method. EMI physics is completely described by Maxwell's four equations, although analytical solutions beyond the simplest geometry are rare due to mathematical complexity.

Our main interest in this article is the frequency dependence of the EMI response. By measuring an object's EMI response in a broad frequency band, we attempt to detect and characterize the object's geometry and material composition. We name this potential new technology exploiting the spectral EMI response *Electromagnetic Induction Spectroscopy (EMIS)*.

For low-frequency geophysical applications, the displacement current resulting from the dielectric property may be ignored up to a megahertz and higher. At zero frequency, we observe the induced magnetism from a permeable (i.e., magnetic) object; this is the foundation of the magnetic method. In this sense, the magnetic method is a subset of the EMI method at zero-frequency with the earth's magnetic field as the inducing source.

From numerous surveys that we have conducted using our multifrequency sensors (GEM-2 and GEM-3; Won et al., 1996 and 1997), we have accumulated significant evidence that a metallic object undergoes continuous changes in response as the transmitter frequency changes. For instance, we have commonly noticed that the observed anomalies have opposite polarities at certain frequencies, depending on whether the target is ferrous or nonferrous. It appears that the phase also depends on the target's geometrical shape. These observations suggest strongly that the EM anomaly measured in a broad band may offer the ability to both detect and identify a target.

Based on elementary EM theory, an object must exhibit different responses at different frequencies. The reason why this fact has not been exploited is due to the lack of practical broadband EMI instruments to study the phenomenon. Most commercial EMI sensors (including common metal detectors) operate at single frequency or, rarely, at a few discrete frequencies. However, with the recent development of the GEM-series sensors, it is now practical to exploit broadband EMI spectra in order to detect and identify the targets.

Because of this spectral limitation, there has been more interest in the "geometrical sounding" method (an expanding transmitter-receiver array at single frequency) than in the "frequency sounding" method (a fixed transmitter-receiver geometry with varying frequencies). We use such sounding methods to obtain enough data to solve for unknown parameters of a preconceived mathematical model. In contrast, EMIS looks for a spectroscopic identity by matching an observed EMI spectrum to a spectrum of known objects.

On the research level, however, there have been many experimental works that studied broadband EMI phenomena. To mention a few, Ryu et al. (1972) measured at 14 discrete frequencies between 200 Hz and 10 kHz with a horizontal loop and measured tilt angle and ellipticity to explore groundwater in California. Ward et al. (1974) tested a similar 14-frequency system between 10.5 Hz and 86 kHz. Won (1980) showed broadband theoretical models and experimental results using a saltwater tank and graphite targets in the labora-
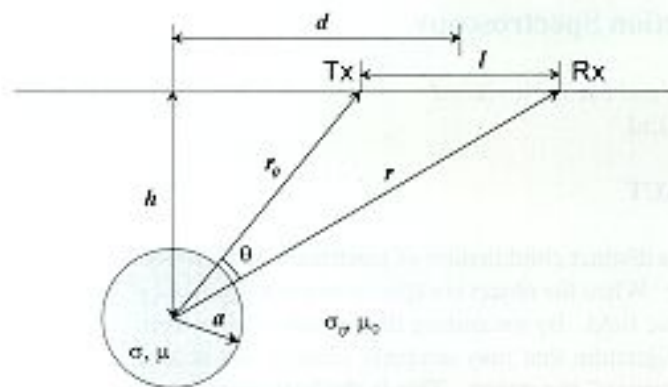
Figure 1. Geometry and notations of a conductive and permeable sphere.

tory. Won (1983) also built and field-tested a prototype sweep-frequency EM system, mounted on a moving vehicle, that automatically measured a continuous frequency response from 100 Hz to 100 kHz.

The new GEM-2 and GEM-3 broadband EMI sensors are suitable for high data-density surveys in a short time with minimal logistics (Won *et al.*, 1996 and 1997). These sensors, weighing about 5 kg each, can measure up to 10 data points per second at multiple frequencies between 90 Hz and 24 kHz, and have a data-logging capacity of about 50,000 points before downloading into a portable computer. From the massive GEM-2 and GEM-3 data we have collected at many different locations over time, we noticed that many buried objects manifest different anomaly polarities at different frequencies. Thus, we suspected the possibility of identifying an object based on its frequency response.

To support the experimental observation, we must first establish a firm theoretical basis for the EMIS concept. In this article, we present the mathematics necessary for some simple models to study theoretically the EMIS response, followed by field examples.

Theoretical Considerations

To explore and understand the EMIS principle, we first consider a solid sphere—a simple object that has an analytic solution under a broadband EM illumination. We want to compute the object's response using combinations of electrical conductivity, magnetic permeability, and sensor geometry with respect to the object and frequency.

Spectral Response of a Conductive and Permeable Sphere

In a series of classical papers, Wait (1951, 1953, 1959, 1960, and 1969) pioneered in deriving the response of a conductive and permeable sphere suspended in whole space. Others (e.g., Fuller, 1971; Lohda and West, 1976) considered more complicated models often involving varying conductivity, layered spherical shells, and conductive host media. The models, however, were commonly investigated to understand the response of mineral deposits for mining exploration and, therefore, their solutions have not been applied to the study of small, manmade, highly conductive and permeable objects in a broad spectral domain.

Let us consider the spectral response of a conductive and permeable sphere excited by a dipole magnetic source. Figure 1 shows the geometry of the problem with the following notations:

m_r or m_θ: radial or transverse dipole moment,
r_o: radial distance of the dipole transmitter,
a: radius of the sphere, and
(r, θ):   the receiver location.

By solving Maxwell's equations with appropriate boundary conditions, one can derive the following spherical harmonics solutions for the secondary magnetic field in the presence of a radial or a transverse magnetic dipole source as depicted in Figure 1. We adopt the expressions and notations used by Grant and West (1965, p. 515), and assume a temporal dependency for all components.

The radial component of the secondary field due to a radial dipole source is given by:
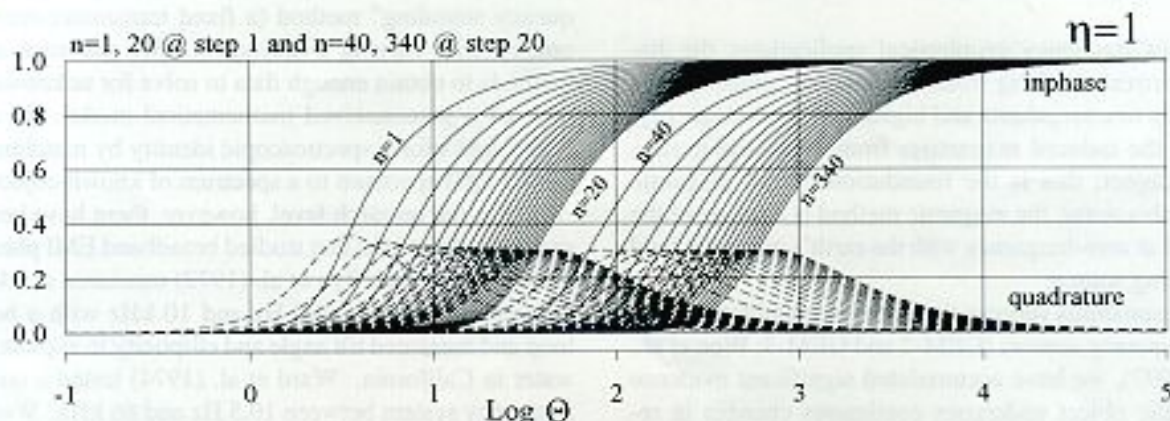

Figure 2. Behavior of X_n and Y_n for an electrically conductive but magnetically nonferrous sphere.
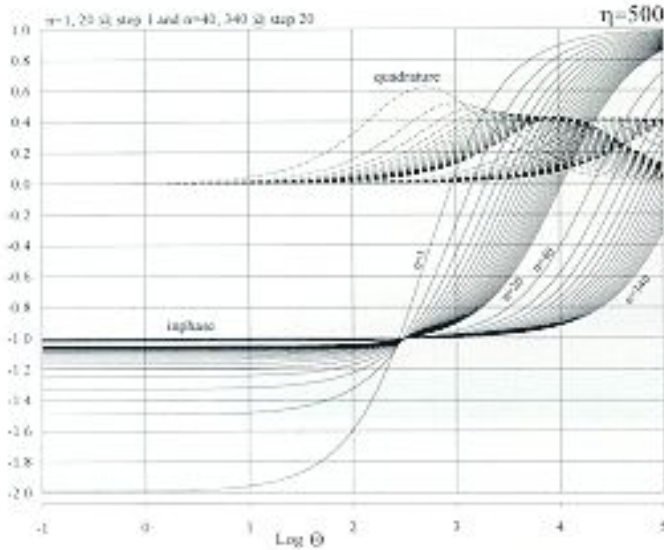
Figure 3. Behavior of X_n and Y_n for an electrically conductive and magnetically permeable sphere.

$$H_{r,r} = -\frac{m_r}{4\pi} \sum_{n=1}^{\infty} (X_n + iY_n) \frac{a^{2n+1}}{(rr_0)^{n+2}} n(n+1) P_n(\cos\theta) \quad (1a)$$

while the transverse component due to a radial dipole source is:

$$H_{r,\theta} = -\frac{m_r}{4\pi} \sum_{n=1}^{\infty} (X_n + iY_n) \frac{a^{2n+1}}{(rr_0)^{n+2}} n P_n^1(\cos\theta) \quad (1b)$$

P_n is the n-th order Legendre polynomial while P_n^1 is the Associated Legendre polynomial. For a transverse dipole, we assume that it always points toward the receiver dipole (fig. 1), which is common to most fixed-geometry EM sensors. For this case, the radial component of the secondary magnetic field is given by:

$$H_{\theta,r} = \frac{m_\theta}{4\pi} \sum_{n=1}^{\infty} (X_n + iY_n) \frac{a^{2n+1}}{(rr_0)^{n+2}} n P_n^1(\cos\theta)$$

$$(1c)$$

while the transverse component due to a transverse dipole is:

$$H_{\theta,\theta} = -\frac{m_\theta}{4\pi} \sum_{n=1}^{\infty} (X_n + iY_n) \frac{a^{2n+1}}{(rr_0)^{n+2}}$$

$$\left\{ n^2 P_n(\cos\theta) - \frac{n}{n+1} \cot\theta P_n^1(\cos\theta) \right\}. \quad (1d)$$

The complex expression $(X_n + iY_n)$ in Eqs. (1a) through (1d), called the *response function*, contains all EM properties and the size of the sphere. The remaining terms, all real, are governed only by the relative geometry between the sphere and the source and receiver locations. The real part of the

response function, X_n, generates the inphase response and the imaginary part, Y_n, generates the quadrature response of the sphere. For a solid, conductive, and permeable sphere, the response function can be shown as:

$$X_n + iY_n = \frac{\left\{ \frac{1}{2} - \eta(n+1) \right\} I_{n+\frac{1}{2}}(ka) + ka \cdot I'_{n+\frac{1}{2}}(ka)}{\left\{ \frac{1}{2} + \eta n \right\} I_{n+\frac{1}{2}}(ka) + ka \cdot I'_{n+\frac{1}{2}}(ka)}$$

$$\text{where } \eta = \mu / \mu_0, \quad (2)$$

in which $k^2 = i\omega\mu_0\sigma$ and

μ_0:   permeability of the host medium,
μ: permeability of the sphere, and
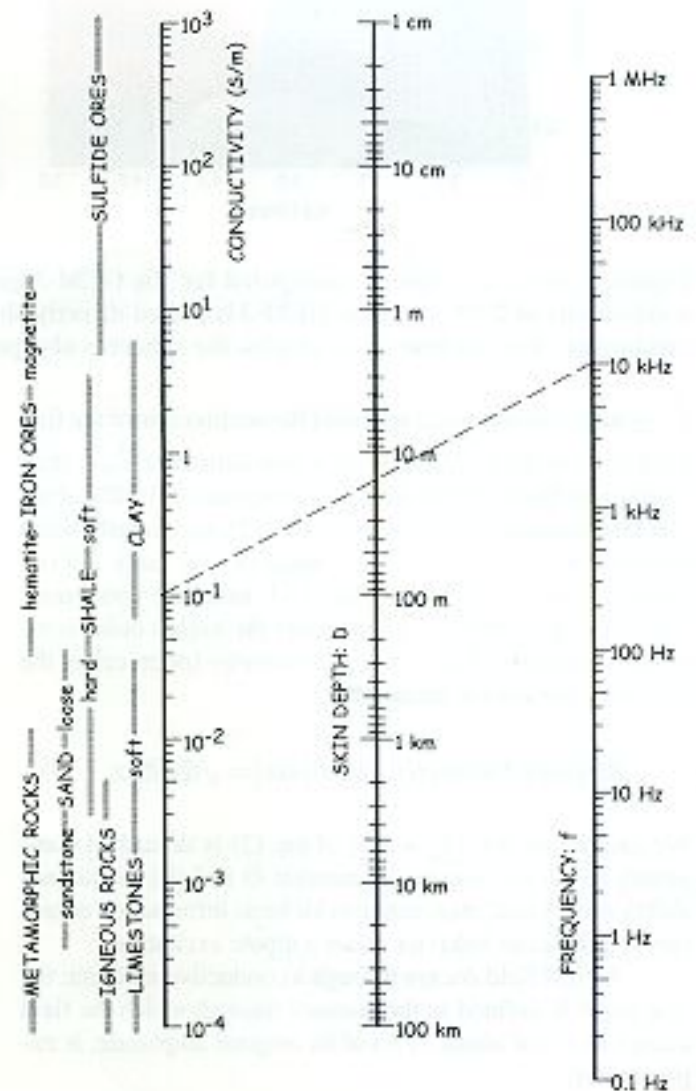σ: conductivity of the sphere.

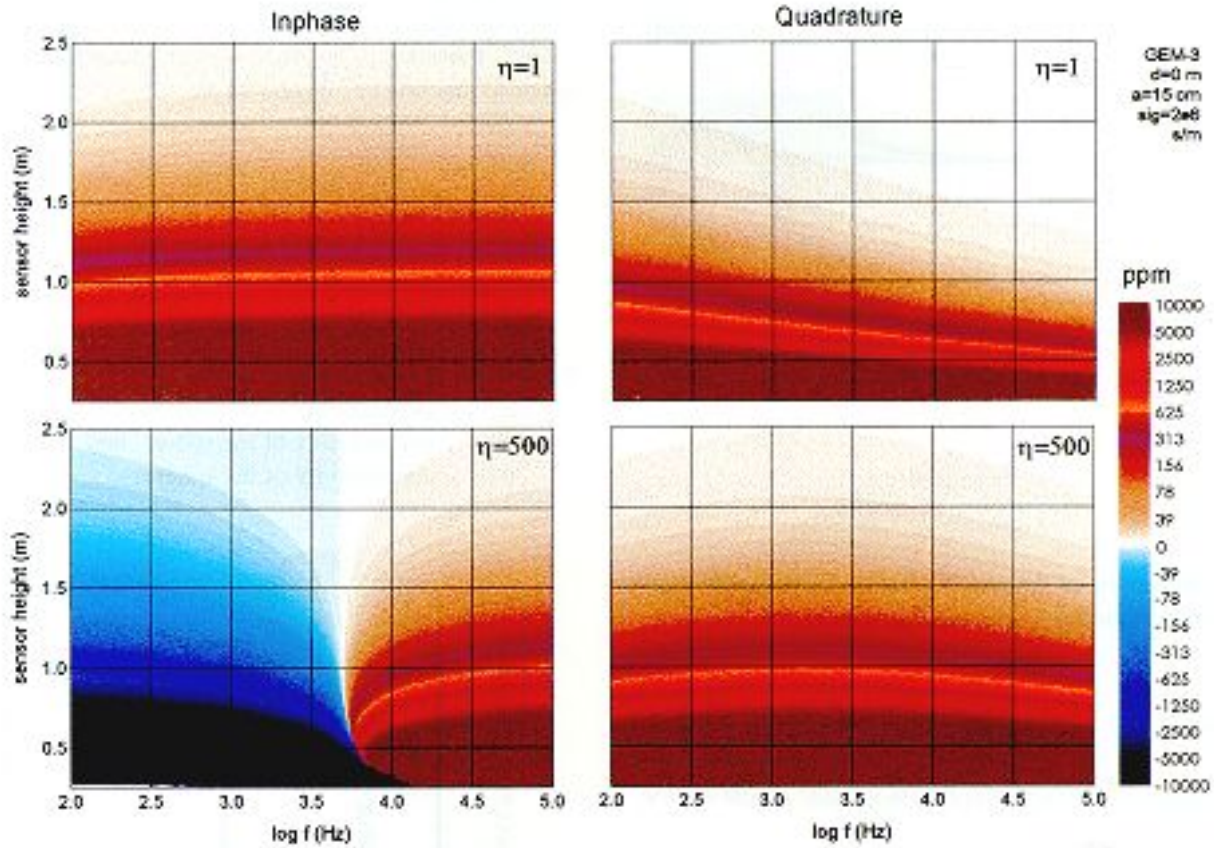Figure 4. Skin depth nomogram (from Won, 1980).

Figure 5. Spectral response (computed for the GEM-3 geometry) of a sphere having a 15-cm radius and a constant conductivity of $2 \cdot 10^6$ s/m. The GEM-3 is placed directly above the sphere. For the upper two graphs, the sphere is only conductive. For the lower two graphs, the sphere is also permeable.

$I_{n+1/2}(ka)$ is the modified spherical Bessel function of the first kind at an order $n+1/2$ and has a first derivative $I'_{n+1/2}(ka)$. Lohda and West (1976) describe computational difficulties and their remedies associated with eq. (2), particularly when the order n is high or ka is very small or very large. In our approach, we computed the ratio I / I' using the continuous fractions representation, which made the higher order computation possible. The *response parameter* (often called the *induction number*) is defined by:

$$\text{Response Parameter:} \quad \Theta = |ka| = \sqrt{\omega\mu\sigma}\, a \quad (3)$$

We emphasize that $(X_n + iY_n)$ of eq. (2) is described completely by (i) the response parameter Θ and (ii) the permeability ratio η and, thus, contains all basic information necessary to predict its behavior under a dipole excitation.

An EM field decays through a conductive medium; the skin depth δ, defined as the distance through which the field decays to e^{-1} (or about 37%) of its original amplitude, is expressed by:

$$\text{Skin Depth:} \quad \delta = \sqrt{\frac{2}{\omega\mu\sigma}} . \quad (4)$$

Eq. (3) now may be written in terms of the skin depth of the sphere:

$$\text{Response Parameter:} \quad \Theta = \sqrt{2}\, \frac{a}{\delta} . \quad (5)$$

Figure 2 shows the computed X_n and Y_n ($n = 1$ to 340) as a function of Θ for the case when the sphere, suspended in free space, is conductive but not permeable (thus $\mu = \mu_0$ or $\eta = 1$). For small Θ (low frequency, resistive limit), both the real (inphase) and imaginary (quadrature) parts are small (thus, little response), but the imaginary part is dominant. For a large Θ (high frequency, conductive limit), the real part is dominant and asymptotically approaches 1. The imaginary part peaks at a particular Θ that is related to the target's physical properties.

Figure 3 shows another case when the target is permeable, having a permeability ratio $\eta = 500$, a representative value for common steels. The quadrature behaves similar to the previous case, while the inphase exhibits large negative
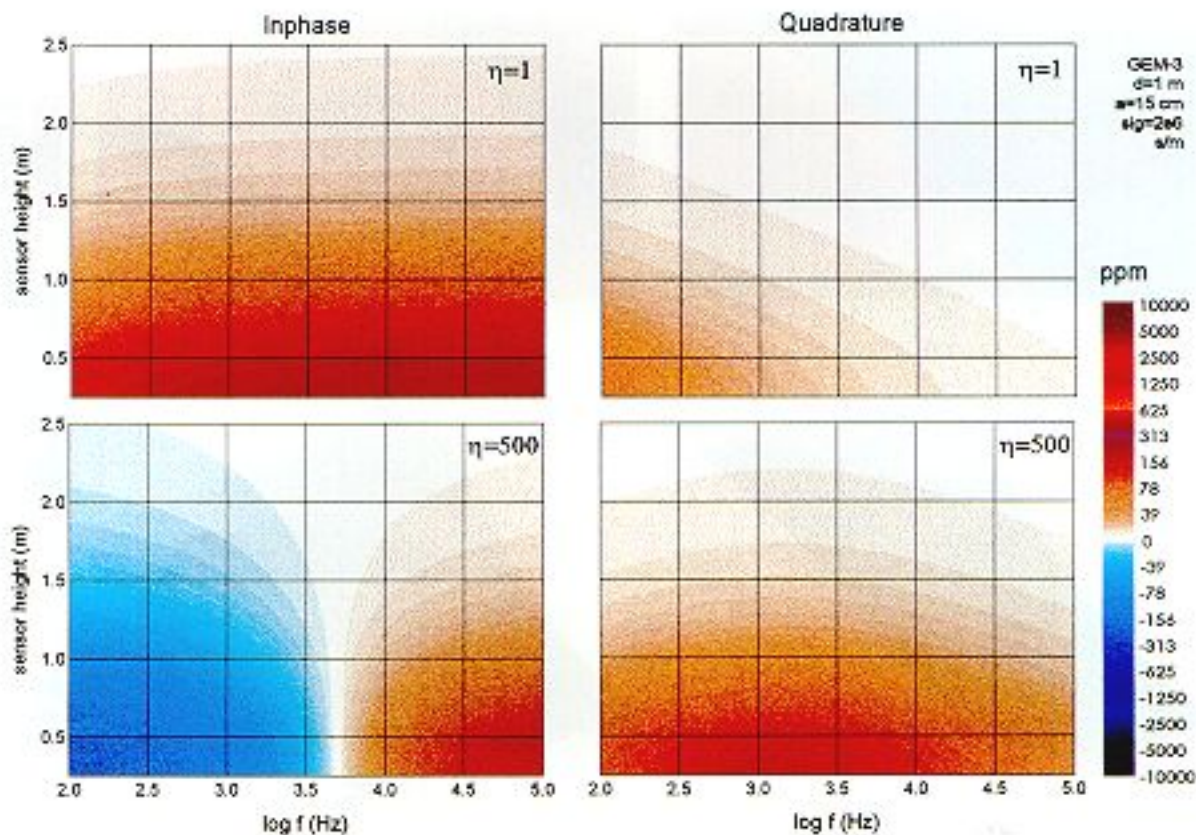
Figure 6. Spectral response (computed for the GEM-3 geometry) of the same sphere as in Figure 5, but the sensor is placed one meter away horizontally from the center. See the text for further details.

values for small Θ. Unlike the conductive sphere of fig. 2, the inphase now is dominant for small Θ. This is the permeability limit at zero frequency, or the DC magnetic response. At a very low frequency, a ferrous sphere is magnetized along the external field lines which, in this case, are generated by a magnetic dipole transmitter. Figure 3 also indicates that the negative inphase changes its sign at a particular Θ for each n and, thereafter, becomes positive as Θ increases. At the crossover, the target becomes invisible in the inphase.

We note in figs. 2 and 3 that both X_0 and Y_0 change considerably when the Θ changes by a few decades. Therefore, if we can measure the response in a broad range of Θ, we should be able not only to detect the sphere but, based upon the observed response, determine its EM properties and geometry as well.

Spectral Response of a Spherical Shell

A spherical shell is also a suitable model for manmade objects. For completeness, we discuss a spherical shell having a finite wall thickness. Similar models were discussed by Wait (1969), Fuller (1971), and others. Assume that the same sphere considered before has a concentric spherical cavity having a radius b. The formal solution is the same as eq. (1a)

through (1d) with the following *response function*:

$$X_A + iY_n = \frac{\varphi_{+a}\left\{\eta(n+1)I_{n-\frac{1}{2}}(kb)-\varphi_{-b}\right\}-\varphi_{-a}\left\{\eta(n+1)I_{n-\frac{1}{2}}(kb)-\varphi_{-b}\right\}-\eta(n+1)}{I_{n-\frac{1}{2}}(ka)\left\{\eta(n+1)I_{n-\frac{1}{2}}(kb)-\varphi_{-b}\right\}-I_{-n-\frac{1}{2}}(ka)\left\{\eta(n+1)I_{n-\frac{1}{2}}(kb)-\varphi_{-b}\right\}+\eta n}$$

(6)

with

$$\varphi_{+a} = \frac{1}{2}I_{n-\frac{1}{2}}(ka) + ka\cdot I'_{n-\frac{1}{2}}(ka),$$

$$\varphi_{-a} = \frac{1}{2}I_{-n-\frac{1}{2}}(ka) + ka\cdot I'_{-n-\frac{1}{2}}(ka),$$

$$\varphi_{-a} = \frac{1}{2}I_{-n-\frac{1}{2}}(ka) + ka\cdot I'_{-n-\frac{1}{2}}(ka), \text{ and}$$

$$\varphi_{-b} = \frac{1}{2}I_{-n-\frac{1}{2}}(kb) + kb\cdot I'_{-n-\frac{1}{2}}(kb).$$

(7)

It is easy to show that as the inner radius $b \rightarrow 0$, eq. (6) becomes identical with eq. (2) for the solid sphere. A similar formula can be derived for a case when the cavity is filled with a different material having another set of EM properties. The response function of a spherical shell is complicated and so is its numerical computation.
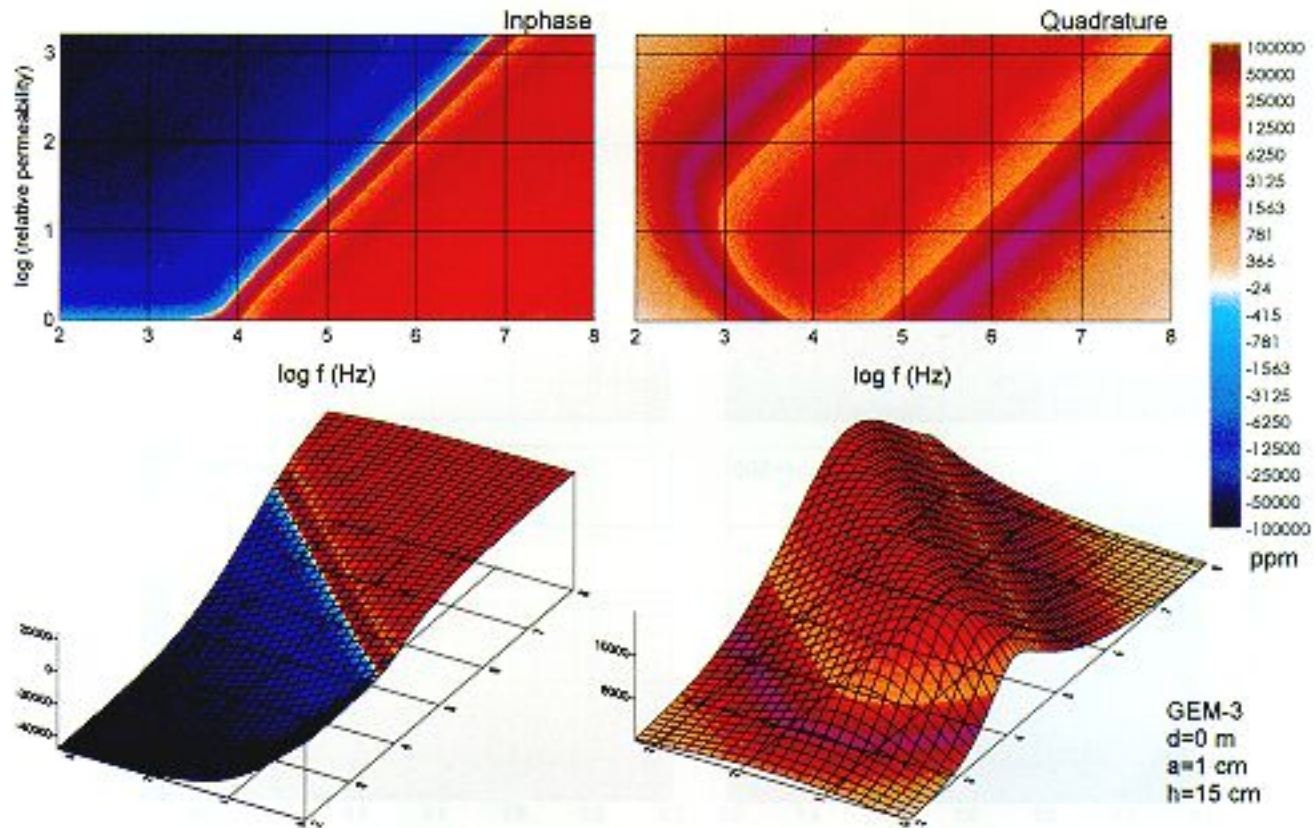
Figure 7. Effect of magnetic permeability for a sphere model having a 1-cm radius, which is placed directly below a GEM-3 at a distance of 15 cm.

Conductivity and Permeability of Common Metals

Because EMIS exploits an object's conductivity and permeability, we briefly review such properties for common metals. The metals used in large quantities for equipment (tools, weapons, etc.), structural strength (beams, rebars, etc.), or packaging (cans, cases, etc.), typically contain iron, aluminum, copper, nickel, and lead. These metals mix in many ways to produce a plethora of metal alloys widely used for daily products from pots and pans to bomb casings. Table 1 shows the electrical conductivity of common metals, which ranges from about 1×10^6 siemen/m (nickel) to about 60×10^6 siemen/m (copper).

Before we look into the magnetic properties of common metals, let us clarify a frequent confusion about the unit of measuring the *magnetic permeability*, which is the ratio between the magnetic induction (B) and the magnetic field strength (H), or $B = \mu H$. When a permeable matter is placed in an existing field H, an induced field is generated inside the matter parallel with H. Combining both fields, we write

$$B = (1 + 4\pi k) H = \mu H \qquad (8)$$

In *emu* units (common in geophysics), B is measured in

gauss and H in oersted, so that becomes oersted/gauss. However, since μ is dimensionless μ in these units, gauss is dimensionally the same as oersted. The *magnetic susceptibility (emu) k* is less than 10^{-3} for most geologic media except for rocks with high magnetite contents.

In MKS units (common in physics and material science), however, the relation is expressed as

$$B = \mu_0 (1 + \chi_m) H = \mu_0 \mu_r H \qquad (9)$$

where μ_0 is the permeability of free space ($4\pi \cdot 10^{-7}$ henry/m), χ_m is again called *magnetic susceptibility* (but 4π times bigger than k), and μ_r is called *relative magnetic permeability*. In these units, B is measured in weber/m^2, and H in ampere-turn/m, and both χ_m and μ_r are dimensionless. Most ferromagnetic materials have very high permeability, so that χ_m and μ_r become numerically the same.

Table 1 shows the magnetic susceptibility (χ_m) for common nonferrous metals. The values are very small; those with small positive values (e.g., aluminum) are called paramagnetic, while those with small negative values (e.g., copper) are called diamagnetic materials.

Table 2 (modified from the CRC Handbook of Chemistry and Physics, 52nd edition) shows commonly used ferro-
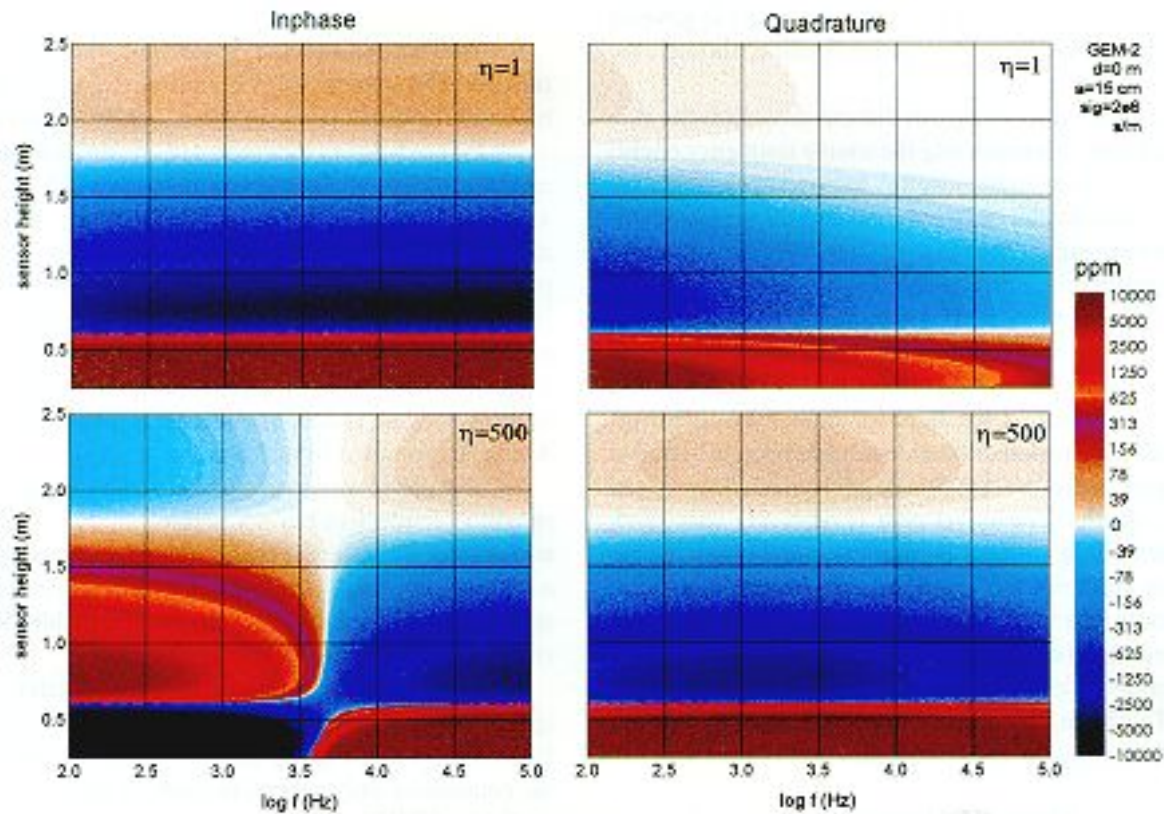
Figure 8. Spectral response (computed for the GEM-2 geometry) of a sphere having a 15-cm radius and a constant conductivity of $2 \cdot 10^6$ s/m. The GEM-2 is placed directly above the sphere. For the upper two graphs, the sphere is only conductive. For the lower two graphs, the sphere is also permeable. See the text for further details.

magnetic metals along with their ranges in μ_r and σ. In comparison with the nonferrous metals (Table 1), the metals in Table 2 show very high μ_r ranging from 100's to 100,000's. It must be noted that the linearity between B and H breaks down for high permeability metals through the hysterisis phenomenon and that μ_r is no longer a constant but depends on the inducing field itself. Although μ_r in Table 2 is shown to be at B=20 gauss (which is about 40 times stronger than the earth field), it still stays within a factor of two or three at a much weaker magnetic field.

The response parameter Θ is a function of frequency, conductivity, permeability, and sphere size. Combining the properties of common metals shown in Tables 1 and 2, we estimate below a probable range of Θ for detecting and characterizing a manmade metallic object:

Parameter	RangeRange in	Decades
1. frequency (e.g., GEM-3)	100 Hz – 30,000 Hz	2.48
2. conductivity (siemen/m)	$(1 - 60) \times 10^6$	1.78
3. permeability (henry/m)	$4\pi \cdot 10^{-7}(1 - 10,000)$	4.00
4. sphere radius	1 cm – 100 cm	2.00
Response parameter Θ: $\{① + ② + ③\}/2 + ④$		*6.13*

The radius range is based on manmade objects such as

landmines and drums. The above estimate indicates that we have potentially over six decades of variations in Θ for ferrous or nonferrous metallic spheres.

Every object containing metals has a distinct conductivity, permeability, and size and shape. These, along with the source frequency, provide a sufficient range of the response parameter for target detection and characterization. Analytic solutions are hard to come by other than for a sphere or a spherical shell; however, it is reasonable to suppose that different shapes would yield different response functions that would help characterize them. The EMIS concept does not require an analytic solution for each object; it identifies an object by empirically matching its measured spectrum against spectra of known objects.

Effect of Burial Depth

For geophysical EMIS applications, we deal with buried objects. We briefly examine here the effect of the earth medium between the surface and the object. A transmitter located above the earth generates an EM field that propagates at a speed of light through the air. Once the field passes into the earth, the wave slows down considerably and it becomes

an almost vertical, highly dissipative plane wave parallel to the earth surface. The skin depth defined by eq. (4) governs the amplitude decay, as well as phase rotation, through the earth.

Figure 4 shows a nomogram that can determine the skin depth (center line) by connecting the source frequency (right) and the medium conductivity (left). Included as a guide are common geologic media and their conductivity ranges. Typical soils have a conductivity range of 0.001 (dry and/or sandy) to 0.1 (wet and/or clayey) siemen/m.

The frequency for EMI instruments, including most metal detectors, rarely exceeds a few hundred kilohertz. As an upper-end example, if we connect 0.1 siemen/m to 100 kHz in fig. 4, we obtain a skin depth of about 5 m. For most EMI methods used to detect small manmade objects buried at shallow depths, therefore, the skin depth is much deeper than the object's depth. The travel path is relatively short and, thus, results in little changes in amplitude and phase during the transit to and from the target through the earth medium. In other words, the majority of the observed EM spectrum from a buried object comes from the object itself and is largely independent of the burial depth or the properties of the earth medium. Therefore, the object's spectral signature will not be affected much by the earth medium.

Theoretical Examples

The response function is independent of the sensor geometry with respect to the sphere. The secondary magnetic field, however, is affected by the relative geometry of the transmitter and receiver (T-R) coils with respect to the sphere. For theoretical examples, therefore, we consider two sensor configurations: the monostatic (or co-located) T-R coils such as for the GEM-3 and bistatic (or separated) T-R coils such as for the GEM-2.

Monostatic Sensor (GEM-3) Theoretical Example

We first consider the case of co-located T-R configuration, for which the GEM-3 is a prime example. The GEM-3 has a bandwidth of 90 Hz to about 24 kHz (Won *et al.*, 1997).

Figure 5 shows the computed GEM-3 anomaly (inphase and quadrature) of a metal sphere having a 15-cm radius and a conductivity of $2 \cdot 10^6$ s/m. The GEM-3 is assumed to be directly above the sphere with the T-R coils in a horizontal plane (i.e., both coils in a vertical-dipole mode). The anomaly is expressed in a unit of parts-per-million or ppm [for details, see Won *et al.* (1997)]. The frequency axis (x-axis) is a log-frequency unit between 2 (100 Hz) and 5 (100 kHz). The vertical axis, the distance between the sphere center to GEM-3, extends from 0.5 m to 2.5 m.

The upper two graphs of fig. 5 show the case when the sphere is conductive but not permeable ($\eta=1$). In the lower two graphs, the sphere is both conductive and permeable with a relative permeability of 500. The difference in spectral response between the two spheres is remarkable. We observe from figs. 5 and 6 the following features:

• The inphase anomaly of a conductive-permeable sphere changes its sign at a specific frequency (the crossover frequency f_c) that slightly depends on the sensor height. For the conductive-only sphere, in contrast, the f_c is too low to be useful for EMIS.

• Below f_c, the inphase polarity is opposite between the conductive sphere and the conductive-permeable sphere. The anomaly polarity alone can distinguish whether the sphere is

Table 1. Electrical and magnetic properties of common nonferrous metals.

	Electrical Conductivity $\times 10^6$ Siemen/m	Magnetic Susceptibility $\times 10^6$ (mks)
Copper	58.82	-9.4
Brass	14.29	-
Aluminum	35.71	21.0
Monel	2.38	-
Lead	4.55	-17.0
Tin	8.70	31.0
Zinc	17.24	-11.4
Nickel	1.28	ferrous
Silver	62.50	-26.0
Gold	40.98	-34.0

Table 2. Electrical and magnetic properties of common ferrous metals.

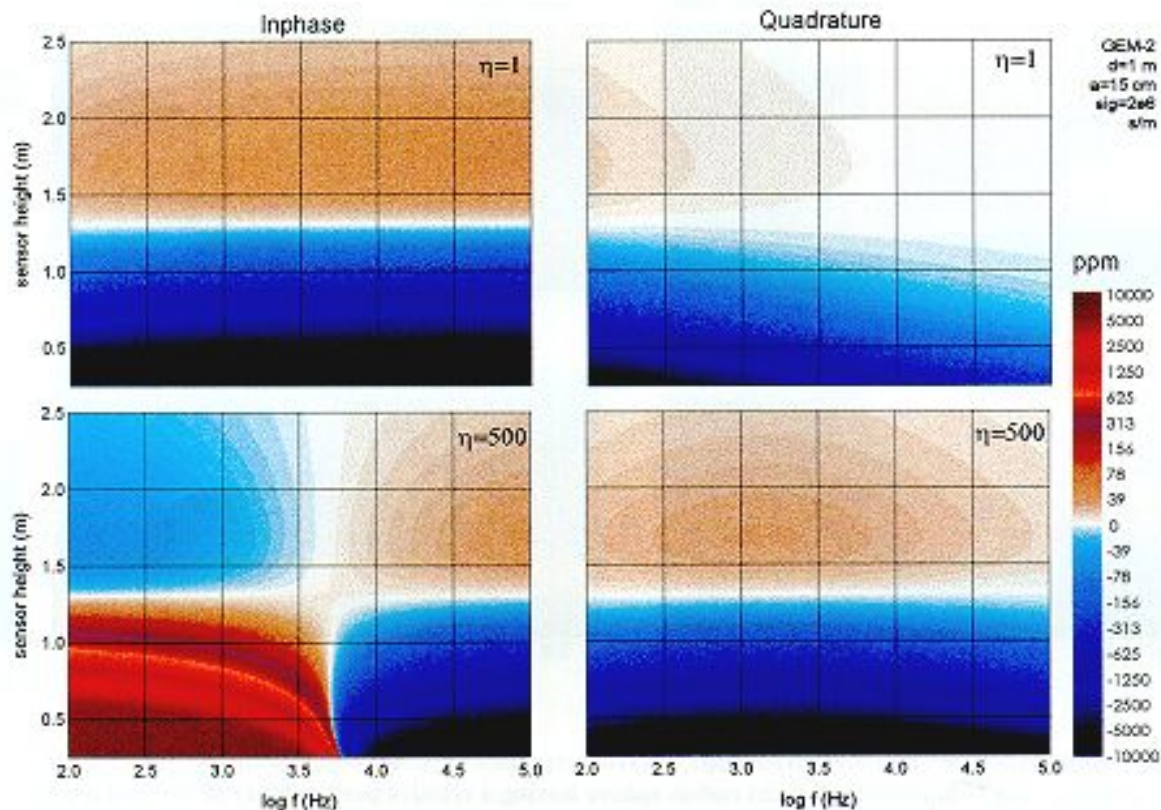|	Electrical Conductivity $\times 10^6$ Siemen/m	Relative Magnetic Permeability @ B=20 Gauss
Cold rolled steel	10.0	100
Iron	10.0	200
Purified iron	10.0	5,000
4% Silicon iron	1.7	500
45 Permalloy	2.2	2,500
78 Permalloy	6.3	8,000
4-79 Permalloy	1.8	20,000
2-81 Permalloy	0.0001	125
Supermalloy	1.7	100,000
Mu Metal	1.6	20,000
Hiperco	4.0	650
Hypernik	2.0	4,500
Monimax	1.3	2,000
Sinimax	1.1	3,000
Permendur	14.3	800
2V Permendur	3.8	800

Figure 9. Spectral response (computed for the GEM-2 geometry) of the same sphere as in Figure 5, but the sensor is placed one meter away horizontally from the center. See the text for further details.

made of a magnetic (e.g., iron) or non-magnetic metal (e.g., aluminum).

•At or near f_c, the sphere becomes invisible to the inphase, which stresses the need for measuring both the inphase and quadrature components. It also implies the necessity of broadband measurements to overcome such blind frequency zones.

•When the sensor is close to the sphere, the f_c is rather sensitive to permeability and, therefore, it can be used to determine the content, or possibly the type, of magnetic material of the sphere. This is an important object identification issue.

•Further target discrimination may be possible by studying the field decay rate in distance or as a function of frequency. Because a sphere with a particular radius, conductivity, and permeability would generate a specific response diagram (fig. 5 as an example), we can fingerprint, at least theoretically, all available spherical objects of interest for comparative identification. All spectral features discussed here can be extrapolated to an object having an arbitrary shape.

Figure 6 shows another theoretical model, when the GEM-3 sensor is placed one meter away horizontally in comparison with the case of fig. 5. The anomalies are attenuated,

but most of the previous observations from fig. 5 still hold.

The effect of magnetic permeability is depicted in fig. 7 using a sphere model having a 1-cm radius, which is placed directly below a GEM-3 at a distance of 15 cm. The response (in ppm units) is shown as a function of frequency (x-axis) for a range of relative permeability between 1 and 2,000. The f_c of inphase response, as well as peak quadrature response, is related to the permeability and sphere size.

Bistatic Sensor (GEM-2) Theoretical Example

We now consider the case of separated T-R configuration, for which the GEM-2 is a prime example. The GEM-2 is a coplanar, bistatic sensor having a T-R separation of 1.6 m. For the construction and operating principle of the GEM-2, refer to Won *et al.* (1996). Having a bistatic T-R geometry, the GEM-2 geometry exhibits more complex spectral response than the GEM-3. We find through modeling that all features observed for GEM-3 are applicable to the GEM-2 case and can be used for spectral target identification.

Figure 8 shows the anomaly (computed for the GEM-2 geometry) of the same sphere as having a 15-cm radius and a conductivity of $2 \cdot 10^6$ s/m.. The midpoint of the GEM-2 T-R
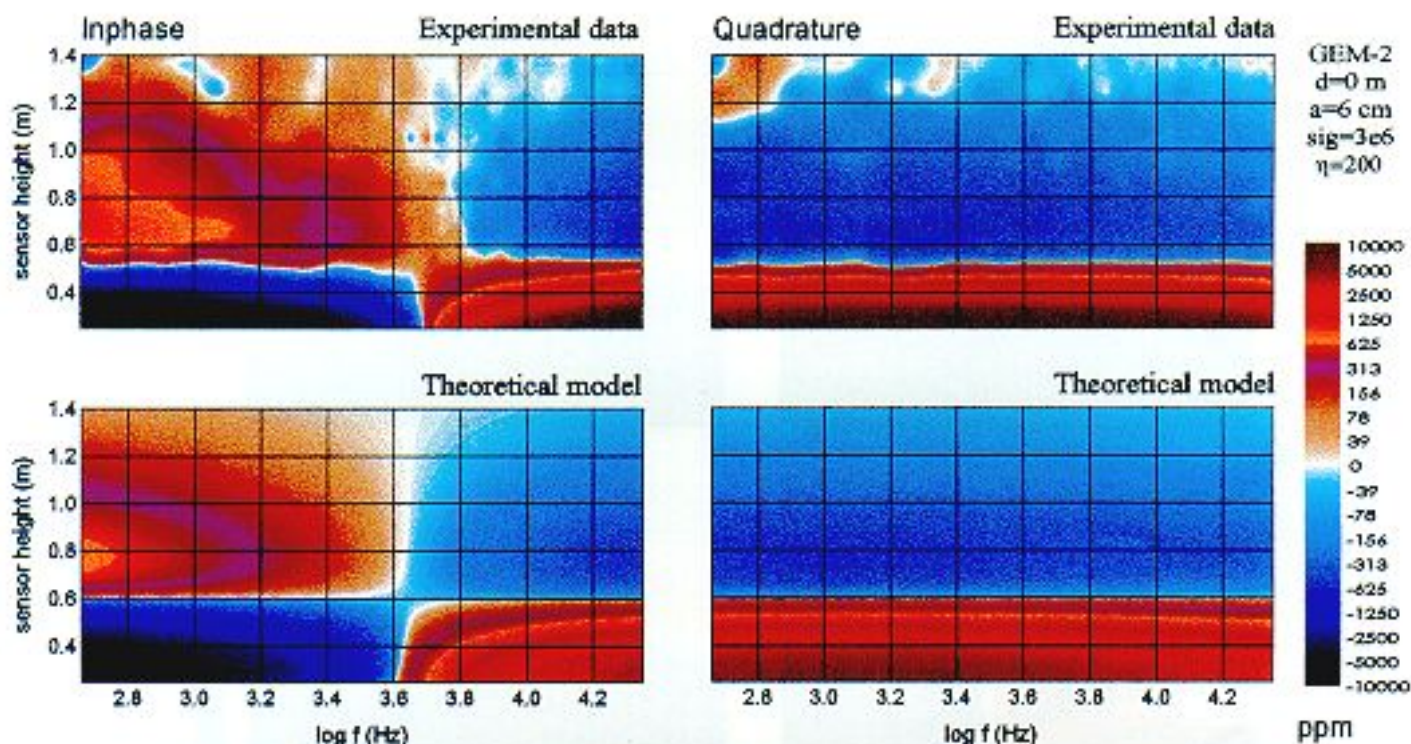
Figure 10. Computed (bottom) and measured (top) spectral responses for a test object using the GEM-2 geometry. The theoretical responses are computed for a 6-cm radius sphere having a relative permeability of 200 and a conductivity of $3 \cdot 10^6$ s/m.

axis is assumed to be directly above the sphere with all coils in a horizontal plane (i.e., vertical-dipole mode). In comparison, fig. 9 shows the case when the GEM-2 is placed one meter away horizontally.

We observe from figs. 8 and 9 the following additional spectral features. The sphere becomes invisible at a certain sensor height (say, the crossover sensor height h_c): 1.5 m in fig. 8 and about 1.05 m in fig. 9. Both the inphase and quadrature change their polarity across h_c, which appears to be independent of either frequency or permeability. From additional models, we find that h_c is also independent of the sphere radius.

In fact, the field equations reveal that, for a given T-R separation of the GEM-2, h_c depends on (i) the sensor offset (d in fig. 1) and (ii) the sphere depth. This is an excellent indicator for determining the target's burial depth. This finding also indicates that a bistatic sensor can be blind to an object at a particular depth, a potential drawback that a monostatic sensor does not have.

Experimental Examples

To verify the predicted spectral responses, as shown in figs. 5 through 9, we conducted an experiment using the GEM-2 and a small object cut from an exercise dumbbell. The ob-

ject, roughly a hexagonal cylinder, has an equivalent radius of about 6 cm when approximated as a sphere. The GEM-2 was run in a sweep-frequency mode to obtain a continuous response spectrum at each sensor height (distance between the GEM-2 and the object), starting from about 20 cm and ending at 2 m. The frequency started at 410 Hz and ended at 24 kHz.

Figure 10 shows, at the bottom, the computed spectral responses for the test object using the GEM-2 geometry. The theoretical responses are computed for a 6-cm radius sphere having a relative permeability of 200 and a conductivity of $3 \cdot 10^6$ s/m. We note a crossover frequency at about 4.1 kHz for the inphase. For the sensor height, we note a distinct crossover at 0.6 m.

On the top of fig. 10, we show the measured responses. The measured signal is strong up to about 1 m and becomes noisy at further distances. Remember, the object is rather small for the GEM-2. The measured responses clearly confirm the theoretical models. We find in general that the field data agrees very well with the computed models.

Figure 11 shows the GEM-3 data at two frequencies (4,050 Hz and 12,270 Hz) over a 62-m by 40-m area in Fort Carson, Colorado. The test site was established by the Defense Advanced Research Projects Agency (DARPA) and the Waterways Experiment Station (WES) to acquire high-den-
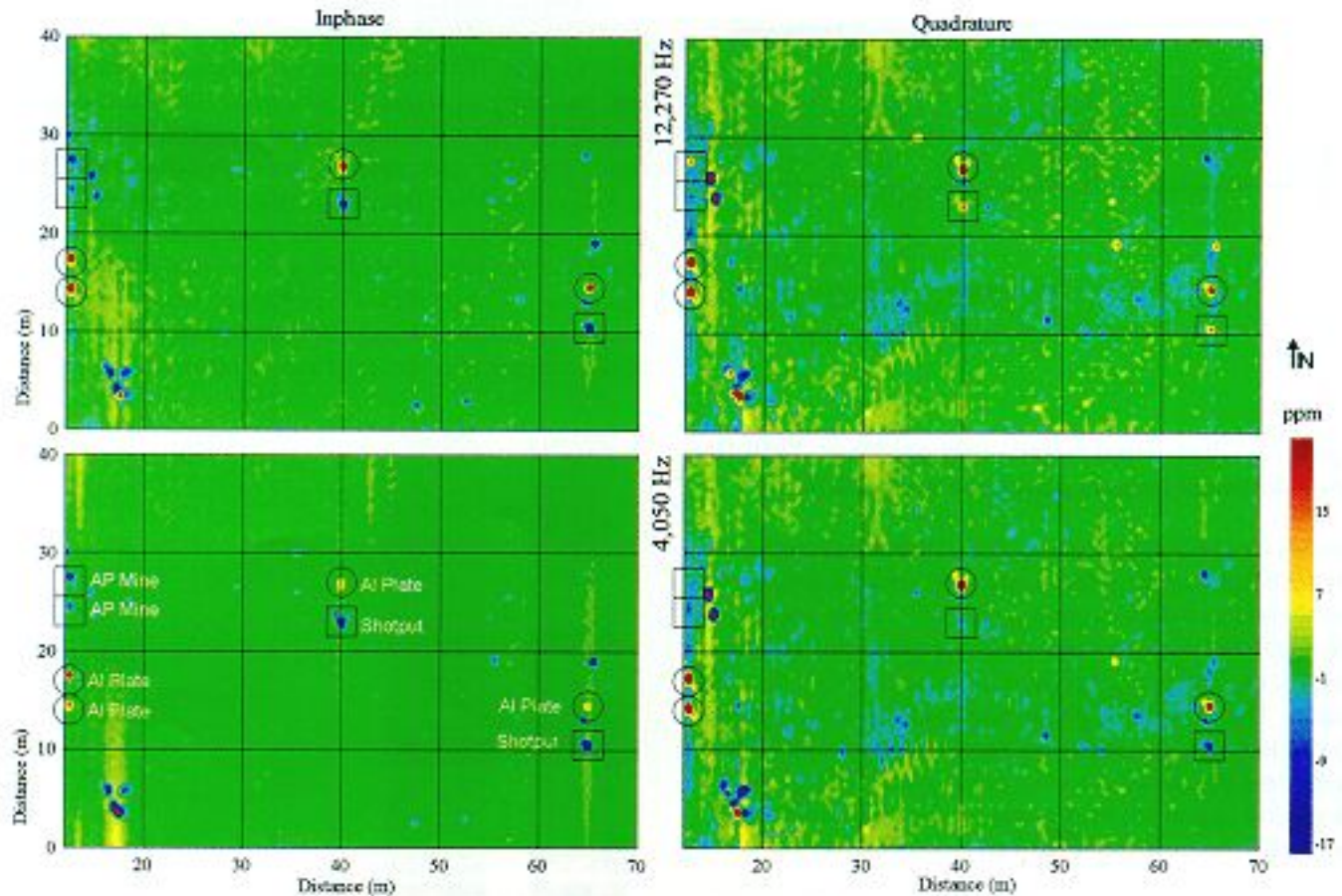
Figure 11. GEM-3 data at two frequencies (4,050 Hz and 12,270 Hz) over a 70-m by 40-m area in Fort Carson, Colorado, where small objects were buried for geophysical tests.

sity data from various geophysical sensors (viz., infrared, magnetic, EM, and GPR) to aid in the detection and discrimination of buried unexploded ordnance and landmines.

Circles and squares in fig. 11 indicate eight known test targets buried in the plot. The four circles indicate aluminum targets; 20-cm by 20-cm and 2.5-cm thick plates. Of the four squares, two are spherical shot-puts (middle and right) having a radius of 6.2 cm. The remaining two are landmines (extreme left); an M14 low metallic AP (antipersonnel) mine and an OZM-3 metallic AP mine.

The aluminum targets are only conductive while the shot-puts are conductive and ferrous. The two landmines contain various amounts of ferrous metals, possibly in addition to small conductors such as copper wires. It is obvious from fig. 11 that there exist many other unknown objects; for instance, six or more objects are around coordinates (15, 5) in the lower left corner.

We collected the GEM-3 data at a 0.5-m line spacing along the N-S direction, the y-axis of fig. 11, which explains the apparent N-S streaks in the contour display. Along each line, the data interval is about 10 cm to 20 cm, depending on the surveyor's walking speed. Figure 12 shows one such N-

S profile (extreme left in fig. 11) of the inphase at 4,050 Hz across the two aluminum plates and two landmines. The anomaly signs alone clearly indicate the difference between conductive and ferrous targets following the theoretical prediction. We observe from figs. 11 and 12 the following additional features:

•All four aluminum plates show positive responses at both frequencies and for both the inphase and quadrature, as they should according to the theory.

•The two shot-puts show strong negative inphase responses at both frequencies, implying that we have not encountered the cross-over frequency in this bandwidth. There is at least one unknown object, at coordinates (15, 4), that changes from a large negative inphase (purple) at 4,050 Hz to a large positive (red) at 12,270 Hz. This object must have the cross-over frequency within this bandwidth.

•The two shot-puts show mostly positive quadrature responses, as they should. At 4,050 Hz, however, at least one shot-put shows a negative quadrature, which may be caused by either (i) wrong calibration of GEM-3 or (ii) the particular ground conditions around this shot-put.

In fig. 13, we show GEM-3 data obtained at ten fre-
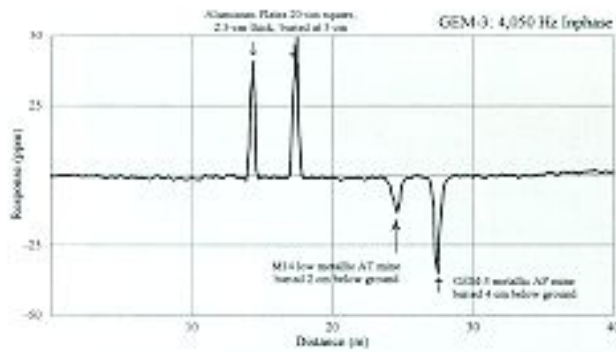
Figure 12. GEM-3 inphase anomaly profile at 4,050 Hz across the two aluminum plates and two landmines.

quencies from 420 Hz (top) to 23,970 Hz (bottom) over a 10-ft by 10-ft test site where six small empty cans were buried on their sides at an 8-inch depth in a clay soil. Three are aluminum soda cans and the other three are steel cans having a similar size. The sensor height is about six inches above the ground. The observed inphase response shows an opposite polarity between the aluminum cans, and steel cans at low frequencies, but comes to a same polarity at high frequencies. The reverse appears to be the case for the quadrature signal. Specifically, we note the following:

Aluminum Cans: The inphase response starts at a very low positive and progressively (and asymptotically) increases with frequency. The quadrature response reaches its highest positive around 5 kHz and diminishes thereafter. The observed response follows the theoretical findings presented in fig. 2.

Steel Cans: The inphase response starts at strong negative but becomes positive at a crossover frequency somewhere between 5 kHz and 11 kHz. The quadrature response becomes highest positive around 11 kHz and slowly diminishes thereafter. The observed response follows the theoretical findings discussed in fig. 3.

It is obvious from the data presented here that broadband EMI data manifest distinct spectral characteristics that can be extremely useful for detecting and discriminating buried objects.

Potential Applications

The concept of EMIS is new and requires a large effort to advance the theoretical understanding and to develop practical hardware and software. As a preliminary step, we suggest the following procedure to apply this concept to a target detection and identification process:

Object Detection: Assume multiple objects buried in a given site, possibly along with false targets that are to be identified as such. The first mission is to detect all potential anomalies, including the target objects, within the site. A multifrequency EM survey (using several frequencies over a broad band) would be most appropriate for detecting anomalies so as to avoid the blind frequency zone (the crossover frequency discussed earlier). Use a GEM-3 type monostatic sensor for small and shallow targets such as unexploded ordnance and landmines. Use a GEM-2 type bistatic sensor for large and deep targets such as drums. Beware that there may be certain sensor heights (the vertical distance between the sensor and
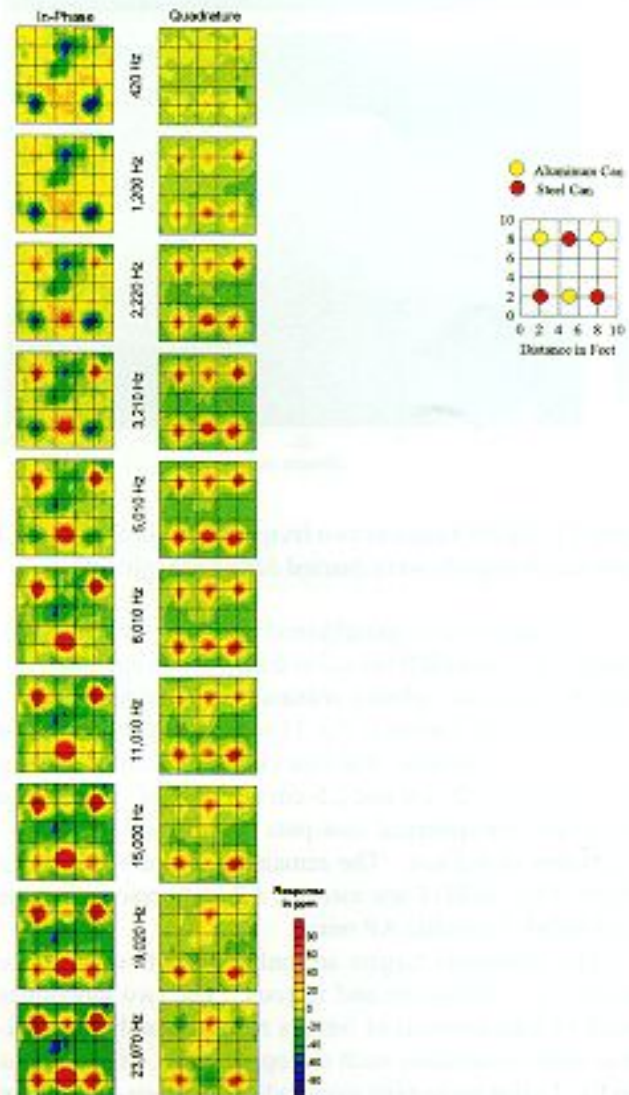
Figure 13. GEM-3 data from 420 Hz (top) to 23,970 Hz (bottom) over a 10-ft by 10-ft test site where six cans (three aluminum soda cans and three steel cans having a similar size) are buried on their sides at a depth of 8 inches in a clay soil. The sensor height is about 6 inches above the ground.

the target) at which the target becomes invisible to the sensor. To overcome this, move the sensor away from the target.

Object Identification and Discrimination: Once a candidate anomaly is located, measure the continuous spectral responses of the object. For the GEM-2 and GEM-3, this can be achieved by either (i) sweeping through the entire bandwidth – a sweep-frequency mode (the operator specifies the start frequency, end frequency, and step interval), or (ii) transmitting a broadband source such as pseudo-random sequence, recording the time-series, and applying the Fourier transform to obtain the response spectrum.

To construct an EMIS plot as in figs. 5 through 9, collect spectral data directly above a candidate object at many different heights. The data can be compared against prerecorded EMIS data for many objects known by their makers and models.

Let us envision an EMIS-based mine detector as an example. In a simple scenario, consider a mine detector that has in its memory the spectral signatures of all known landmines. The detection phase can be accomplished using a few discrete frequencies that are chosen to be optimal for a given geologic and cultural environment. Once a target is suspected, we start the identification phase that involves recording the target's spectral response. The measured spectrum may be scanned through the signature memory in order to identify a particular landmine or, if no match is found, reject the target as a not-a-mine item. A given minefield would likely contain only one or, at most, a few types of mines, which would considerably reduce the computational effort. In addition, as the search progresses, the sensor may be able to develop its own artificial intelligence for improved discrimination.

Conclusions

The purpose of EMIS is to detect and identify hidden metallic objects that can be characterized by their electrical conductivity, magnetic permeability, and geometrical size and shape. To realize fully its potential as a new technology, we need to further develop broadband EMI models and advanced sensor hardware and software.

EMIS technology may be particularly useful for detecting buried landmines and unexploded ordnance. By characterizing and identifying an object without excavation, we should be able to reduce significantly the number of false targets. EMIS should be fully applicable to many other problems where the target identification and recognition (without intrusive search) are important. For instance, an advanced EMIS device at an airport security gate may be able to recognize a particular weapon by its maker and type.

Acknowledgements

References

Grant, F. S., and West, G. F, 1965, Interpretation Theory in Applied Geophysics, McGraw-Hill Book Co., New York, 584 p.

Fuller, B. D., 1971, Electromagnetic response of a conductive sphere surrounded by a conductive shell, *Geophysics*, **36**, p. 9-24.

Lodha, G. S. and West, G. F., 1976, Practical airborne EM (AEM) interpretation using a sphere model, *Geophysics*, **41**, p. 1157-1169.

Ryu, J., Morrison, H.F., and Ward, S.H., 1972, Electromagnetic depth sounding experiment across Santa Clara Valley, *Geophysics*, **37**, p. 351-374.

Wait, J. R., 1951, A conducting sphere in a time-varying magnetic field, *Geophysics*, **16**, p. 666-672.

Wait, J. R., 1953, A conducting permeable sphere in the presence of a coil carrying an oscillating current, *Canadian Jour. Physics*, **31**, p. 670-678.

Wait, J. R., 1959, Some solutions for electromagnetic problems involving spheroidal, spherical, and cylindrical bodies, *J. Res. N.B.S.* (Mathematics and Mathematical Physics), **64B**, p. 15-32.

Wait, J. R., 1960, On the electromagnetic response of a conducting sphere to a dipole field, *Geophysics*, **25**, p. 619-658.

Wait, J. R., 1969, Electromagnetic induction in a solid conducting sphere enclosed by a thin conducting spherical shell, *Geophysics*, **34**, p. 753-759.

Ward, S. H., Pridmore, D. F., Rijo, L., and Glenn, W. E., 1974, Multispectral electromagnetic exploration for sulfides, *Geophysics*, **39**, p. 662-682.

Won, I. J., 1980, A wide-band electromagnetic exploration method: some theoretical and experimental results, *Geophysics*, **45**, p. 928-940.

Won, I. J., 1983, A sweep frequency electromagnetic method, Chapter 2 in *Development of Geophysical Exploration Method - 4*, Editor A.A. Fitch, Elsevier Applied Science Publishers, Ltd., London, p. 39-64.

Won, I. J., Keiswetter, D. A., Fields, G. R. A., and Sutton, L. C., 1996, GEM-2: a new multifrequency electromagnetic sensor, *Jour. Environmental and Engineering Geophysics*, Vol. 1, No. 2, p. 129-138.

Won, I. J., Keiswetter, D. A., Hanson, D. R., Novikova, E.,

and Hall, T. M., 1997, GEM-3: a monostatic broadband electromagnetic induction sensor, *Jour. Environmental and Engineering Geophysics*, Vol. 2, Issue 1, p. 53-64.